



## Full length article

## Development of a novel imaging agent using peptide-coated gold nanoparticles toward brain glioma stem cell marker CD133

Jun-Haeng Cho<sup>a</sup>, A-Ru Kim<sup>a</sup>, Sang-Heon Kim<sup>a</sup>, Su-Jae Lee<sup>b</sup>, Hoeil Chung<sup>a</sup>, Moon-Young Yoon<sup>a,\*</sup><sup>a</sup> Department of Chemistry and Research Institute of Natural Sciences, Hanyang University, 222 Wangsimni-ro, Seongdong-gu, Seoul 133-791, Republic of Korea<sup>b</sup> Department of Life Science, Hanyang University, 222 Wangsimni-ro, Seongdong-gu, Seoul 133-791, Republic of Korea

## ARTICLE INFO

## Article history:

Received 5 May 2016

Received in revised form 28 September 2016

Accepted 5 October 2016

Available online 6 October 2016

## Keywords:

Phage display

Peptide

CD133

Cancer stem cells

Gold nanoparticles

## ABSTRACT

CD133 is known as biomarker for glioblastoma (GBM) and also serves as a marker for cancer stem cells (CSCs), which carry out tumorigenesis and resist conventional therapeutics. The presence of CD133-presenting CSC is a one of the factors in maintenance of the tumorigenic potential of GBM. Thus, CD133 is a potential target for accurate diagnosis of GBM, which could improve its poor prognosis for patients when CSCs are present.

Herein we designed a small peptide-based imaging agent with stimulus-responsive properties. A novel small peptide, CBP4, was screened by a phage display technique, and demonstrated binding to the target CD133 (ECD) comparable to that of an antibody. As a quencher, we used gold nanoparticles (GNPs); the targeting peptide was conjugated to GNPs with high efficiency. By means of a quenching effect, the peptide-coated GNP showed ‘signal on–off’ properties depending upon the presence of the target. In addition, the particles exhibited biocompatibility when localized in the cytosol. Thus, this study demonstrated that the peptide-coated GNPs can be utilized as an imaging agent for accurate diagnosis of GBM, and further as a drug carrier for therapeutic approaches.

## Statement of Significance

The diagnosis and determination of prognosis made by cancer stem cell markers could be a key strategy to eradicate cancer stem cells and cure the cancer. The significance of this study is the characterization of quenching-based signal on–off mechanism and showed that the active targeting via peptide can contribute to the design of a stimulus-responsive cellular imaging agent. Moreover, small peptide based nano complexation showed specific recognition of the target stem cell and internalized on cellular cytosol with stimulus responsive fluorescence. With its novel biocompatibility, the strategy might be a promising tool for drug carrier systems able to measure and visualize the delivered efficiency at intracellular sites.

© 2016 Acta Materialia Inc. Published by Elsevier Ltd. All rights reserved.

## 1. Introduction

Brain tumors are one of the most feared types of cancer, inducing dysfunctions in the neural circuitry and having poor prognosis when malignant. Glioblastoma (GBM), as the most common type of primary malignant brain tumor, has only a 16- to 18-month median survival rate when multimodal treatment is applied [1]. Despite increasing knowledge of the genetic and molecular characteristics of GBM, therapeutic efficacy has only slowly improved over the past decade [2]. Several studies have shown that the presence of cancer stem cells (CSCs) was one of the factors in the self-

renewal of cancer cells to promote tumor growth after conventional GBM therapy [3,4].

CSCs have been identified in various malignant types of cancer, including leukemia and solid tumors [5]. Because they can be self-renewing and pluripotent, CSCs have been indicated as a cause of tumor initiation, metastasis, and drug resistance [6].

CD133 is known as a cell surface antigen allowing identification of CSCs in various types of solid tumors including GBMs [7]. In brain tumors, the existence of CSCs was first assayed using CD133 with their prospective isolation and CD133<sup>+</sup> CSCs showed stem cell properties including self-renewal and metastasis [8]. Further, it was reported that the CD133 cell surface antigen helps increase the population of tumor initiating cells and has an essential role regarding the maintenance and tumorigenic potential of

\* Corresponding author.

E-mail address: [myyoon@hanyang.ac.kr](mailto:myyoon@hanyang.ac.kr) (M.-Y. Yoon).

GBM [9,10]. Therefore, CD133 was one of the effective cell surface biomarkers for accurate diagnosis of GBM.

In the present study, we designed a novel target-specific imaging system targeting CD133 as a glioma biomarker. Toward this end, we screened the peptide using the M13 phage library. Phage display has been used to identify a small molecule with target-specific recognition properties using a library of  $10^9$  random complexity [11]. A random genomic sequence was inserted into the expression vector and cloned using the M13 phage virus to form a phage library at a p3 minor coat protein [12]. Through various screening techniques, the peptide motif as the product possess strong binding affinity to various targets including proteins, hormones, and cells [13]. As a tool for diagnostic systems, peptides have several advantages over antibodies. Peptides, owing to their smaller size (1–3 kDa), show greater penetration of cells and tissues than antibodies [14]. Further, relative to antibodies, peptides have comparable binding affinity, are less immunogenic, less toxic, and simpler to produce [15]. Hence, peptides have various clinical applications and are considered as promising alternatives to antibodies [16].

In the present work, toward the development of a target-specific imaging system based on a small peptide, we prepared citrate-capped gold nanoparticles (GNPs). GNPs have been used widely in visualization and biological imaging systems to identify specific agents, and have several advantages such as biostability, simplicity of synthesis, ease of surface modification and conjugation with biomolecules, and novel optical properties [17,18]. In addition, GNPs have strong fluorescence quenching ability, as much as 100 times that of conventional quenchers [19]. The FRET quenching mechanisms of GNPs have been used as the basis for many prospective biological sensing systems targeting various molecules, from DNA to macromolecules [20,21]. Stimulus-responsive nanocomplexation has been used as a technique to apply GNPs in an imaging system for disease diagnosis [22].

Especially in the tumor microenvironment, various physical and chemical cellular conditions including enzymatic reactions [23], cellular pH [24], and redox reactions [25] and these have attracted interest in the development of stimulus-responsive nanomaterials for antitumor applications. The tripeptide glutathione ( $\gamma$ -glutamyl-L-cysteinyl-glycine; GSH) has been identified as an agent that has a cleaving mechanism and exists within tumor cells. GSH is synthesized in cellular cytosol from its precursor amino acids. It has an important role in controlling the cellular cycle and microtubule-related reactions, and acts as a reducing agent in various cellular signaling pathways [26]. In cancer cells, GSH is particularly involved in regulating mutagenesis, DNA synthesis, cell growth, and drug resistance, and also protects the cell against oxidative stress. The drug resistance mechanism of malignant cancer cells is frequently associated with higher levels of GSH than would occur in normal tissue [27]. Nano complexation triggered by GSH has been reported as a promising tool for drug and gene delivery to intracellular targets [28]. This tool relies on the fact that the amount of GSH in intracellular organelles is much higher (5–20 mM) than in extracellular fluids (2–20  $\mu$ M) [29]; it has also been reported that GSH is of significantly higher concentration in tumor cells than in normal cells [30]. Through the formation of sulfur bonds [31], GSH can enhance the secretion efficiency of delivered and released therapeutic biomolecules within tumor cells [32].

Herein, we designed the novel stimulus responsive imaging tool for detection the brain glioma stem cell. (Fig. 1) To this, we initially identify a novel small peptide that specifically recognizes CD133. This peptide exhibits a specific localization property on cellular cytosol by means of receptor-mediated endocytosis, as observed from confocal microscopy conducted under live cell conditions. Further, the peptide was conjugated with gold nanoparticles as a

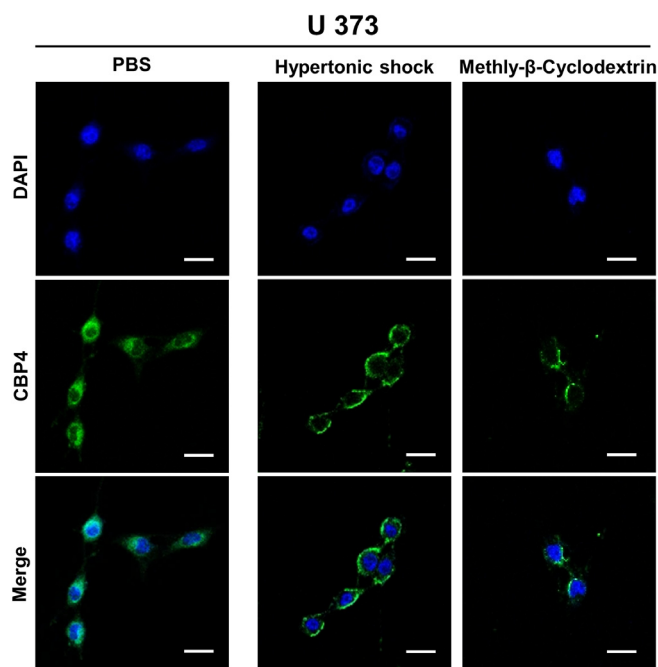


**Fig. 1.** Endocytic assay using CBP4 on U373 glioma cells. FITC-labeled CBP4 was incubated with U373 human glioma cells for 1 h at 37 °C, followed by laser scanning confocal microscope imaging. Scale bar: 20  $\mu$ m.

quenching agent, and the conjugate's stimulus-responsive characteristics were studied in the presence of GSH as the stimulus agent. We finally confirmed the novel fluorescence 'signal on-off' property of the peptide-coated gold nanoparticles as an imaging agent for glioma.

## 2. Methods

### 2.1. Immunocytochemistry analysis

U373 glioma cells were used for ICC analysis. The cells were trypsinized with 0.25% trypsin and counted at  $0.5 \times 10^5$  cells/well. The cells were grown overnight in a tissue culture dish ( $35 \times 10$  mm<sup>2</sup>) in 5% CO<sub>2</sub> atmosphere at 37 °C. After incubation, the medium was aspirated and the plate was washed three times using PBS. The cells were pre-incubated with a blocking buffer containing 5% FBS to minimize nonspecific binding. The CBP4, which screened by in vitro M13 phage display (Supporting information), was diluted to 100 nM concentration using a binding buffer (pH 7.2, 50% FBS). In the case of the antibody specific to CD133, the antibody was directly incubated with the cells for 6 h at 4 °C. After incubation, the cells were washed three times using PBS, and nucleus staining was carried out by incubating the cells with 4,6-diamidino-2-phenylindole (DAPI). As a negative control, HEK293T cells were also tested using CBP4 under the same conditions. Finally, the cells were washed three times with PBS and mounted with Dako mounting medium. Stained cells were visualized with a fluorescence microscope (Olympus IX71).

### 2.2. Sphere cell formation and immunostaining analysis

The U373 glioma cell was subcultured using sphere-forming medium as described previously [33]. A conditioning medium containing epidermal growth factor, (20 mg/mL), fibroblast growth factor (20 mg/mL), and B27, and not containing FBS, was used for sphere formation. For immunostaining of tumor spheres, a 24-well plate was precoated by means of treatment with poly-d-

lysine (PDL, 150–300 kDa) of 0.00125% concentration overnight at 4 °C [34]. After incubation, the well was washed twice using PBS, and then washed twice with distilled water (dH<sub>2</sub>O). The cells in DMEM were subcultured using conditioning medium and grown overnight in a CO<sub>2</sub> incubator. The sphere cells were transferred to a PDL-coated 24-well plate and incubated for 4 h in a CO<sub>2</sub> incubator to immobilize them. After immobilization, the cells were washed once with PBS and the cells were fixed by adding 4% paraformaldehyde and incubating for 40 min. The solution was aspirated and the cells were washed twice with PBS. To compare the binding efficiency of CBP4 and antibody, probes of 500 nM were added to each well and incubated for 8 h at 4 °C with gentle shaking. Nucleus staining and measurement were carried out as described above.

### 2.3. Inhibition of endocytosis

The U373 cells were trypsinized with 0.25% trypsin and counted to  $0.25 \times 10^5$  cells, and then seeded on a 96 well plate. The cells were grown overnight in a tissue culture dish ( $35 \times 10 \text{ mm}^2$ ) in 5% CO<sub>2</sub> atmosphere at 37 °C. The U373 glioma cells were pre-treated with hypertonic buffer (50 mM HEPES, 140 mM NaCl, 2.5 mM MgCl<sub>2</sub>, 1 mM CaCl<sub>2</sub>, 3 mM KCl, and 450 mM sucrose) for 1 h at 37 °C. This hypertonic buffer was also used in all washing and incubation steps. The cells were incubated with hypertonic buffer containing 500 nM of CBP4 for 1 h, and were then washed three times. Cell fixing and nucleus staining were carried out as described above. The stained nuclei were visualized using confocal microscopy (Leica TCS SP5). The cells were also treated using methyl- $\beta$ -cyclodextrin (M $\beta$ CD) to investigate the endocytic property of the interaction between CD133 and CBP4. The cell was incubated with 6 mg/ml of M $\beta$ CD for 1 h to minimize the decrease in cell viability in a 5% CO<sub>2</sub> atmosphere at 37 °C. Afterward, the cell was incubated with the indicated concentration of CBP4 for 1 h. The visualization process was the same as described above.

### 2.4. Quantification of conjugated CBP4 using dithiothreitol

The quenching effect between the FITC on the CBP4 and the GNPs was assessed from absorbance and fluorescence spectra after treatment with dithiothreitol (DTT) as a strong redox agent [35]. First, DTT was reacted with GNP-PEG-CBP4 and GNP-PEG to analyze the dissociation efficiency. To samples of 5 nM GNP solution, various concentrations of DTT were added and incubated for 1 h at room temperature with rotation. To separate the reactant, the mixture was centrifuged at 12,000 rpm for 30 min, and the process was repeated twice to minimize nonspecific quenching signals. The supernatant was transferred to fresh tubes for measurement of fluorescence intensity. The pellet was resuspended in dH<sub>2</sub>O for measurement of absorbance spectra. To allow fluorescence measurement in the linear response region, the FITC-labeled CBP4 samples were diluted serially and measured.

### 2.5. Stimulus-response assay

Glutathione (GSH) was used to estimate the stimulus-response properties of GNP-PEG-CBP4. Solutions containing GNP-PEG-CBP4 were centrifuged at 12,000 rpm for 30 min. The supernatant was removed from each sample and the pellets were resuspended in six different media: (a) PBS (pH 6.0) containing 10 mM GSH, (b) PBS (pH 6.0) containing no GSH, (c) PBS (pH 7.4) containing 10 mM GSH, (d) PBS (pH 7.4) containing no GSH, (e) PBS (pH 8.0) containing 10 mM GSH, and (f) PBS (pH 6.0) containing no GSH. Subsequently, samples of the media containing GNP-PEG-CBP4 were incubated at 37 °C and removed for testing in a time-dependent manner. To terminate the reaction, the mixture was

centrifuged at 12,000 rpm for 20 min to separate the dissociated GNP from the FITC-labeled peptide. After centrifugation, the supernatant was transferred to new tubes and the centrifugation step was repeated. The stimulus-responsive property of the GNP-PEG-CBP4 conjugates was also tested in various concentrations of GSH; the procedure used was the same as described above. The fluorescence of the final supernatant was analyzed using the Soft Max V5 system.

### 2.6. Monitoring the fluorescence recovered efficiency

As a target, U373 glioma cells were counted to  $0.25 \times 10^5$  on each plate. HEK293T cells were also incubated as a negative control. The counted cells were incubated overnight in a 5% CO<sub>2</sub> atmosphere at 37 °C. Under live cell conditions, various concentrations (6, 8, 10, and 15 nM) of GNP-PEG-CBP4 and GNP-PEG solution including 50% medium were added to each cell culture plate. After incubation time (6, 8, and 10 h), the reaction was terminated by aspirating the probe complex and washing the cell plate three times with PBS. The cells were fixed by adding 4% paraformaldehyde and incubating at room temperature for 1 h. The fixed cells were washed 3 times using PBS and the cellular nuclei were stained with DAPI solution for a 5 min incubation period with gentle shaking. Fluorescence images were measured in the same way as described above. As a control, 15 nM GNP-PEG-CBP4 (without FITC) and GNP-PEG-scPeptide (scramble peptide) were also incubated for 8 h.

### 2.7. Estimation of cellular internalization of GNP-PEG-CBP4

The hypertonic buffer used in this step was of the same composition described above. The single CBP4 was also tested as positive control. Briefly, cells ( $0.25 \times 10^5$  cells/well) were grown overnight and washed once with hypertonic buffer. As a baseline condition, PBS was used for the dilution and washing steps. To inhibit the endocytosis of CD133, the cells were incubated with hypertonic buffer for 1 h at 37 °C in 5% CO<sub>2</sub> atmosphere under live cell conditions. GNP-PEG-CBP4 of 15 nM was added to cells including 50% medium and incubated for 8 h at 37 °C in 5% CO<sub>2</sub> atmosphere. CBP4 of 500 nM was also incubated for 1 h as a baseline condition. After incubation, the cells were washed using washing buffer and the cells were fixed using 4% paraformaldehyde. The cell fixing and nucleus staining processes used were the same as described above. The stained nuclei were visualized using confocal microscopy (Leica TCS SP5). M $\beta$ CD was also used as a general endocytosis inhibitor. Various concentrations (2, 4, and 6 mg/ml) of M $\beta$ CD were used in this experiment. The M $\beta$ CD was incubated with cells for 1 h to minimize the reduction of cellular viability. After incubation, the cell was washed 3 times using PBS, and 15 nM of GNP-PEG-CBP4 was incubated for 8 h in a 5% CO<sub>2</sub> atmosphere at 37 °C. The visualization process was the same as described above.

### 2.8. Statistical analysis

The data were analyzed using one-way ANOVA, and the significance levels of  $p < 0.05$  and  $p < 0.005$  are reported herein.

## 3. Results

### 3.1. Gene cloning and protein purification

Using an enzyme digestion test, we were able to confirm that the target CD133 ECD coding gene was ligated to the expression vector (Fig. S1a, b). The plasmid DNA was transformed to BL21 (DE3) competent cells and expression was induced using IPTG

under overnight incubation at 18 °C. The target protein was purified, using denaturing conditions to purify the insoluble form of the target protein. The purified recombinant protein showed high homogeneity in 12% SDS-PAGE gel electrophoresis (Fig. S1c, d). The purified protein was incubated with dialysis buffer in a semipermeable membrane overnight at 4 °C. The concentration of the purified protein was 0.39 mg/L, as determined by the Bradford assay method.

### 3.2. Phage display and characterization

The phage display technique used is illustrated schematically in Fig. S2. After four rounds of biopanning, we randomly picked 40 plaques for identification of the genomic sequence. The clones of the selected phage were categorized into four groups according to their amino acid sequence as expressed in the P3 phage coating protein. Table S2 summarizes the screening results. The selected phages were assessed for binding affinity and specificity as follows. First, the CD133 binding phage (CBP) was prepared and the concentration of each phage was determined in terms of plaque-forming units per volume. The screened phages had comparable binding affinities ( $K_d^{app}$ ) for CD133 ECD in the picomolar ( $10^{-12}$ ) range; CBP4 had stronger binding affinity than the others (Fig. S3a). In addition, the specificity was also tested using various negative control proteins: CD44, HER2, and BSA. CBP1 had a stronger CD133 binding signal than the other phages, but also had a greater extent of nonspecific binding. CBP2 and 3 showed weaker binding than the other phages, to both the target CD133 and the negative control. CBP4 had more potent binding to the target CD133 and its binding signal toward the negative control was less than that of the other phages. (Fig. S3b). Accordingly, we selected CBP4 for use as a novel peptide probe toward CD133 and as a subject for further characterization.

### 3.3. Characterization of synthetic peptides

The binding affinity and specificity of synthetic peptides was measured by means of fluorescence assay. CBP4 had a strong binding affinity toward the target, with a  $K_d$  value of 5.5 nM (Fig. S4a). Notably, the  $K_d^{app}$  of the FITC-conjugated peptide was observed to be 20-fold that of the phage-displayed peptides. However, compared with the antibody, CBP4 had novel binding capacity as a diagnostic probe (Table S3). In the specificity test, CBP4 exhibited a strong fluorescence signal in the presence of the target CD133 and not in the presence of the negative control, CD44, HER2, or BSA. (Fig. S4b). We also analyzed the binding affinity of CBP4 to the target U373 glioma cells. As negative controls, we selected HEK293T cells, which rarely express CD133 on the cell surface, as well as FBS and BSA. CBP4 showed strong binding to the target cell U373 only, with a corresponding  $K_d$  value of 1.6  $\mu$ M. This result showed that the CBP4 specifically recognized the target at the cellular level (Fig. S5).

### 3.4. Immunocytochemistry

U373 glioma cells were stained using CBP4 to confirm the targeting efficiency; green fluorescence was observed on the CBP4-stained cells (Fig. S6a). The anti-CD133 antibody and scramble peptide were also tested on a cell stained as a control. In the case of the scramble peptide, only a weak nonspecific signal was observed compared with those of the CBP4 and the anti-CD133 antibody. In addition, the CBP4 gave a similar signal as the antibody. The binding signal was also tested on the HEK293T cells as a negative control. No fluorescence signal was observed for the HEK293T cells, indicating the specific recognition property of the CBP4. The sphere cells were also stained using CBP4 and antibody

(Fig. S6b). The CD133 expression level, which is a cancer initiating marker, was enhanced when sphere cells were formed [36]. The stained result show that the CBP4 and antibody exhibited similar fluorescence binding signals on the target cells.

### 3.5. Cellular internalization efficiency of CBP4

To analyze the internalization efficiency of CBP4 as a mediator for stimulus-response imaging of GNP-PEG-CBP4, we stained the cells using CBP4 under hypertonic and M $\beta$ CD treatment conditions [37,38]. During inhibition with endocytosis conditions, confocal images revealed that CBP4 was specifically localized on the cellular membrane, not the inner cytosol (Fig. 1). In contrast, CBP4 was localized in both the cytosol and the membrane under baseline conditions. The cellular internalization of CBP4 was blocked by inhibition of CD133 based receptor mediated endocytosis. To investigate the biocompatibility of CBP4, we measured its cytotoxicity using MTT (3-(4,5-Dimethylthiazol-2-yl)-2,5-Diphenyltetrazolium Bromide) and a Propidium iodide (PI) staining method. When cells were incubated under a high concentration of CBP4 (1  $\mu$ M), their viability was unaffected (Fig. S7). Overall, the CBP4 showed cellular internalization properties via CD133-mediated endocytosis and were biocompatible at the cellular level.

### 3.6. Characterization of GNPs

Optical properties of the synthesized GNPs were analyzed by means of absorbance spectroscopy. The absorbance peak maximum of the GNPs was observed at the wavelength of 520 nm (Fig. 2a). The GNPs were also analyzed structurally by means of SEM, which showed that the particles were tightly distributed in size (Fig. 2b, c). By means of a Gaussian fitting model, the mean particle size was calculated to be  $14.7 \pm 0.06$  nm. The final concentration of synthetic GNPs was calculated to be 15 nM ( $9.03 \times 10^{15}$  - particle/L). To optimize the stability of the GNPs, they were reacted with various molar ratios of CM-PEG-SH. Self-aggregation of GNPs induced by NaCl was a standard condition used to determine whether the GNPs were PEGylated [39]. GNPs were not aggregated when molar ratios greater than 1 by 3750 were used in the PEGylation. However, after the use of lower molar ratios, the GNPs were aggregated directly when NaCl was added, with the color changing to red to dark purple (Fig. 2d). We thus selected the 1 by 3750 M ratio as optimal for the PEGylation of GNPs.

### 3.7. Conjugation of CBP4 on PEGylated GNP and quantification thereof

CBP4 was conjugated with surface carboxyl groups of PEGylated GNPs (GNP-PEG) by means of the EDC/NHS crosslinker. The absorption maximum of the GNPs shifted bathochromically as a result of the ligand capping; this occurred because ligand capping leads to variation of the GNPs' surface plasmons [40]. To confirm the CBP4 conjugation, we measured the absorbance spectra of GNP-PEG-CBP4 and GNP-PEG to determine whether there was any spectral shift. The peak absorbance wavelength of the GNP-PEG-CBP4 was 2–3 nm greater than that of the GNP-PEG control (Fig. S8). To quantify the conjugation, we applied DTT as a reducing agent toward GNP-PEG-CBP4. The fluorescence of the separated supernatant was saturated when 2.5 mM DTT was used as a reducing agent (Fig. 3a). Contrastingly, no fluorescence from GNP-PEG was observed after its reaction with DTT. A calibration curve of CBP4 was prepared (Fig. 3b), according to which the concentration of conjugated CBP4 was  $1.2 \pm 0.2$   $\mu$ M (70–80%) on 5 nM GNPs. After separation of the supernatant of the reaction with DTT, the pellet was also measured to analyze the optical properties of the GNPs therein. The remaining GNP solution was self-aggregated by means

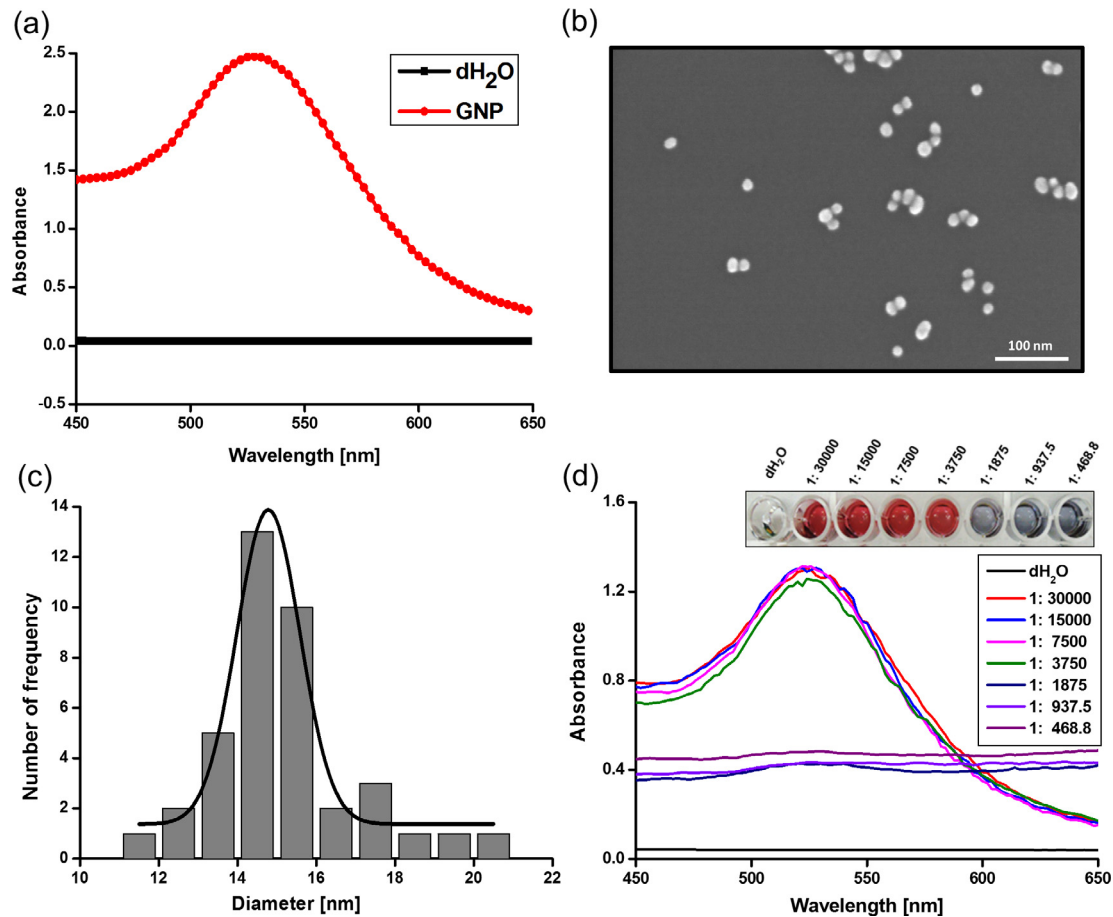


**Fig. 2.** Characterization of synthetic GNPs: (a) absorbance spectra of GNPs, (b) SEM image analysis, (c) size distribution analysis, (d) absorbance spectra analysis to check for NaCl-induced self-aggregation, and images showing colorimetric changes of GNPs.

of thiol–thiol interactions under high concentrations of DTT (Fig. 3c, d).

### 3.8. Analysis of fluorescence quenching

To confirm the fluorescence quenching between FITC on CBP4 and GNPs (Fig. 4a, b), we collected fluorescence and absorbance spectra. The absorbance spectra showed that the optical characteristics were maintained in both GNP-PEG-CBP4 and GNP-PEG. The peak shift resulting from CBP4 conjugation was evident in both samples. The sample of CBP4 alone did not show any absorbance peak variation (Fig. 4c). The supernatant collected after the DTT displacement reaction was separated to measure the fluorescence of the detached CBP4, and the fluorescence of the non-reacted GNP-based solution was also measured at the same time. In the case of GNP-PEG-CBP4, the fluorescence signal was increased by the detachment of CBP4 via DTT, and the signal corresponded to 1.3  $\mu\text{M}$  CBP4. Contrastingly, no fluorescence increase was observed for the supernatant of GNP-PEG, with or without exposure to DTT (Fig. 4d).

### 3.9. Stimulus-response properties (GSH)

The dissociation of CBP4 from GNPs was measured using GSH, which has reductive activity. To optimize the release conditions, PBS buffers of various pH were used as reaction buffers. In the presence of GSH, the fluorescence was increased owing to detachment of CBP4 from GNPs (Fig. 5a). Especially, in acidic reaction conditions (PBS, pH 6.0) including 10 mM GSH, the displacement

was more efficient than in buffer of higher pH. A weak fluorescence signal was also observed from the buffer with no GSH. The decreased stability of GNP-PEG-CBP4 can affect the dissociation of CBP4 from GNP during long-term exposure to the incubation temperature of 37  $^{\circ}\text{C}$ . The displacement efficiency was saturated when 10 mM of GSH (PBS, pH 6.0) was reacted with the GNP-PEG-CBP4 under 10 h of incubation at 37  $^{\circ}\text{C}$  (Fig. 5b). The GNP-PEG-CBP4 exhibited 60–70% cumulative release under 10 mM GSH as compared to that under the baseline condition of DTT.

### 3.10. Monitoring the fluorescence recovered efficiency

Cellular imaging was carried out to analyze the fluorescence response of GNP-PEG-CBP4 in the presence of a stimulating agent in cytosol. We tested the response under various concentrations of GNP-PEG-CBP4 and after various incubation times (Fig. S9). No recovered fluorescence was observed under the 4 and 6 h incubation conditions except in the case in which cells were incubated with 15 nM GNP-PEG-CBP4. Under the 8 h incubation condition, the conditions of 6 nM and 8 nM of GNP-PEG-CBP4 yielded weak fluorescence signals in response to the GSH stimulus. Contrastingly, the cells incubated with 10 nM GNP-PEG-CBP4 showed a weak fluorescence signal at 6 h and a stronger signal at 8 h. Under 8 h incubation condition using 10 nM GNP-PEG-CBP4, the fluorescence signal was stronger than in the 6 nM and 8 nM condition. The cellular fluorescences were also observed after incubations of 4, 6, and 8 h under 15 nM GNP-PEG-CBP4. The fluorescence signal of GNP-PEG-CBP4 was specifically distributed throughout the cellular cytosol and not on the cell membrane. To confirm the speci-

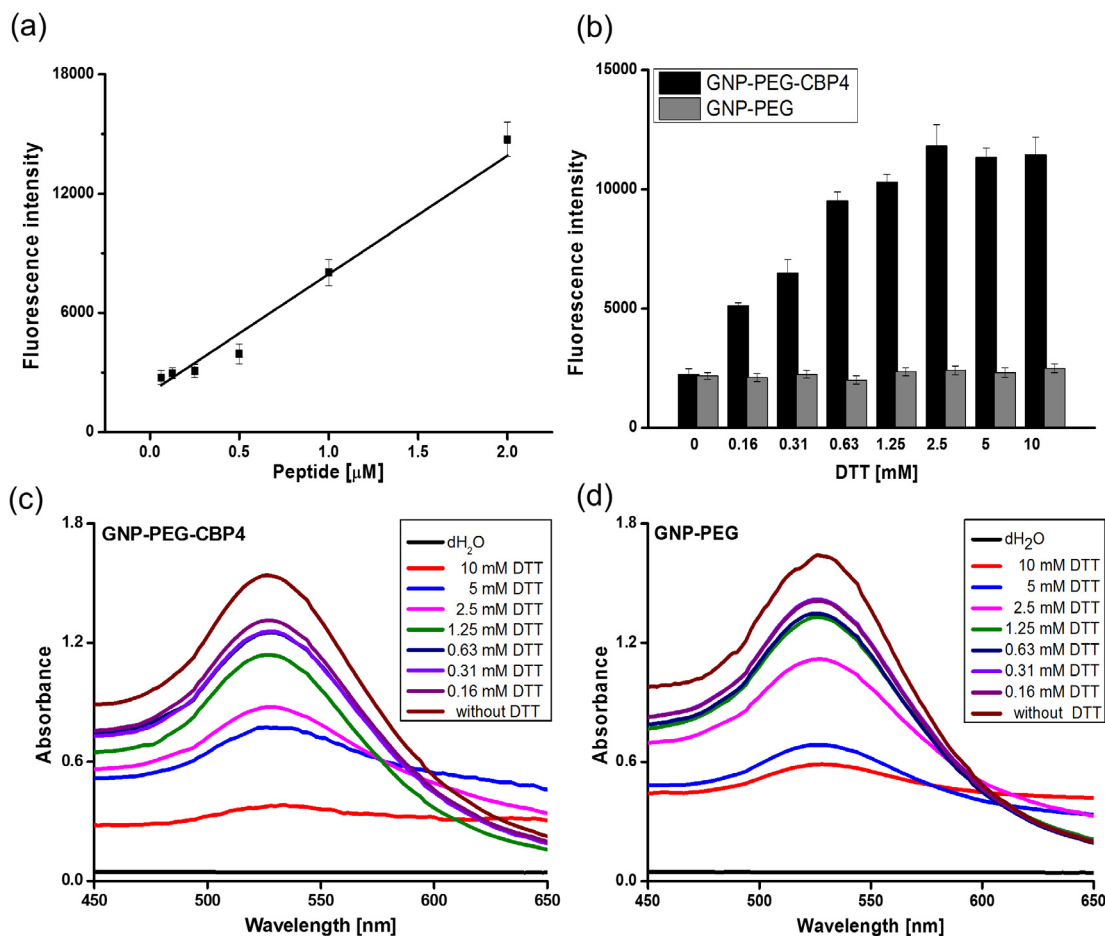


**Fig. 3.** Quantification of peptides conjugated on GNPs. (a) Linear calibration of CBP4. Solid black squares indicate the mean values of three individual measurements for the respective concentration, error bars represent the standard error of deviation, and the solid line represents the linear regression of the mean value ( $R^2 = 0.94$ ). (b) Fluorescence recovery efficiency measurement of GNP-PEG-CBP4 and GNP-PEG; DTT was used as a displacement reagent at the indicated concentration. (c, d) Absorbance spectra for DTT displacement products of (c) GNP-PEG-CBP4 and (d) GNP-PEG.

ficity of GNP-PEG-CBP4, HEK293T cells were tested as a negative control. Only weak and nonspecific signals were observed when 15 nM GNP-PEG-CBP4 were incubated with the control cells for 8 h. The immunostaining results are summarized in Fig. 6. We also synthesized CBP4 without FITC and the peptide with the scramble sequence to compare the specific imaging property of GNP-PEG-CBP4 via active targeting (Fig. S10a). Stimulus-recovered fluorescence occurred only when CBP4 bound to the CD133 protein on the U373 cell (Fig. S10b). This result additionally implies that the binding characteristics of the CBP4 peptides were maintained despite their conjugation with the nanoparticles.

### 3.11. Estimate the cellular internalization efficacy of GNP-PEG-CBP4

We tested the internalization efficiency of GNP-PEG-CBP4 using hypertonic buffer and M $\beta$ CD on U373 cells. CBP4 alone was tested as a negative control at the same time. Strong fluorescence was observed as a response to the cellular stimulus of GNP-PEG-CBP4 under the baseline condition (Figs. 7, S11). Especially, the fluorescence was specifically localized on cytosol, the same as CBP4 under the baseline condition. Contrastingly, under inhibition of endocytosis condition, the endocytosis of CD133 was blocked and thus the GNP-PEG-CBP4 was not internalized in the cell, resulting in a lower chance of exposure to the stimulus agent than in the baseline condition. The weak fluorescence shown in hypertonic

conditions mainly arose because the effect of the hypertonic buffer weakened during the long incubation period.

### 3.12. Cytotoxicity assay

Cell viability was assessed by means of MTT assay and a PI staining method to analyze the biocompatibility of GNP-PEG-CBP4. To measure the mitochondrial dehydrogenase activity, the target U373 cells were incubated with various concentrations of GNP-PEG-CBP4; a PBS and dimethyl sulfoxide (10%) were also used as controls. GNP-PEG-CBP4 had no cytotoxic effect on the target cells at concentrations up to 15 nM (Fig. 8(a)). The cytotoxicity was measured using CBP (1  $\mu\text{M}$ ), GNP-PEG (15 nM) and GNP-PEG-CBP4 (15 nM) for various incubation times (8, 10, and 12 h). The GNP-PEG-CBP4 did not affect cellular viability at any of the incubation times studied. In addition, the result of PI staining demonstrated that the probes do not affect the cellular viability (Fig. 8(c)). In both experiments, the calculated cell viability for GNP-PEG-CBP4 was the same as that for PBS, indicating that GNP-PEG-CBP4 is biocompatible as a cell imaging agent.

## 4. Discussion

CD133 was first identified as a marker for cancer-initiating cells in brain tumors and as a contributor to CSCs, which carry out tumorigenesis and resist conventional therapeutics. Also, CD133

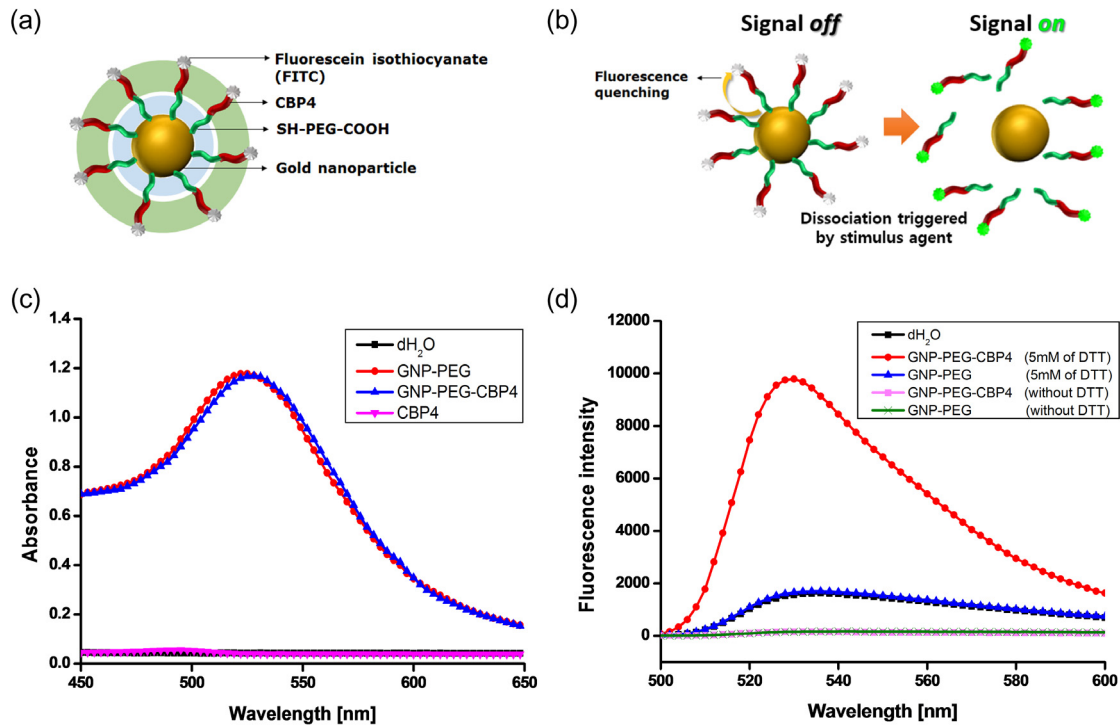


**Fig. 4.** Analysis of the quenching effect of FITC on CBP4 and GNPs. Schematic of the (a) gold nanoparticle and surface groups and (b) fluorescence activation and quenching of GNP-PEG-CBP4 triggered by a stimulus agent. (c) Absorbance spectra of GNP-PEG, GNP-PEG-CBP4, and CBP4. (d) Fluorescence spectra for reacted products of GNP-PEG-CBP4 and GNP-PEG, and for non-reacted solution.

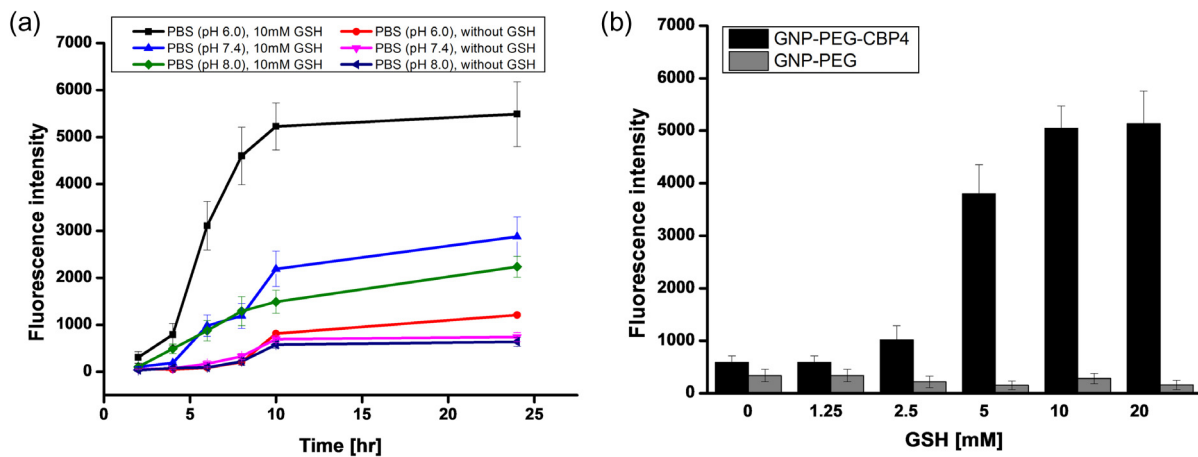


**Fig. 5.** Response of GNP-PEG-CBP4 to GSH stimulus. (a) Time-dependent fluorescence intensity measurements in various buffers in the presence of 10 mM GSH. (b) Determination of saturated fluorescence recovery from quenching by means of measurement under various molar concentrations of GSH after 10 h of incubation.

is known as a marker for CSCs in GBM, the most malignant type of brain tumor in adults, and its presence is a key factor in the maintenance of the tumorigenic potential of GBM. Therefore, accurate detection of CD133 might be a promising technique for improving the poor prognosis for patients suffering from GBM.

In the field of disease diagnosis, marker-specific antibodies have usually been used as detection probes [41]. However, antibodies have several limitations as applied in diagnostic systems including imaging systems, kits, and sensors [42]. To overcome the limitations, we used a M13 phage library to screen the small peptides of 12-mer amino acids toward CD133 membrane protein. From the highly complex library, CBP4 was selected and possessed strong binding potency to the target CD133 and to CD133-presenting cells also (Fig. S5). Especially, CBP4 had binding affinity

( $K_d^{app}$ ) comparable to that of the antibody (Table S3). In addition, CBP4 specifically recognized the target CD133 in vitro at the cell level, and not the control HEK293T cells (Fig. S6). We tested the binding efficiency of CBP4 to sphere U373 cells, which have higher CD133 expression levels [43]. A fluorescence image was observed as a result of the CBP4 staining, confirming the binding efficiency of the screened signal CBP4.

As a receptor protein, CD133 has an endocytic property when the ligand binds to its extracellular surface [44]. To estimate the cellular internalization efficiency of CBP4, we used hypertonic buffer and M $\beta$ CD, which is known as an inhibitor for endocytosis [45]. Under live cell with inhibition conditions, confocal imaging revealed that CBP4 was specifically localized on the membrane and not in the cytosol. Contrastingly, under the baseline condition,

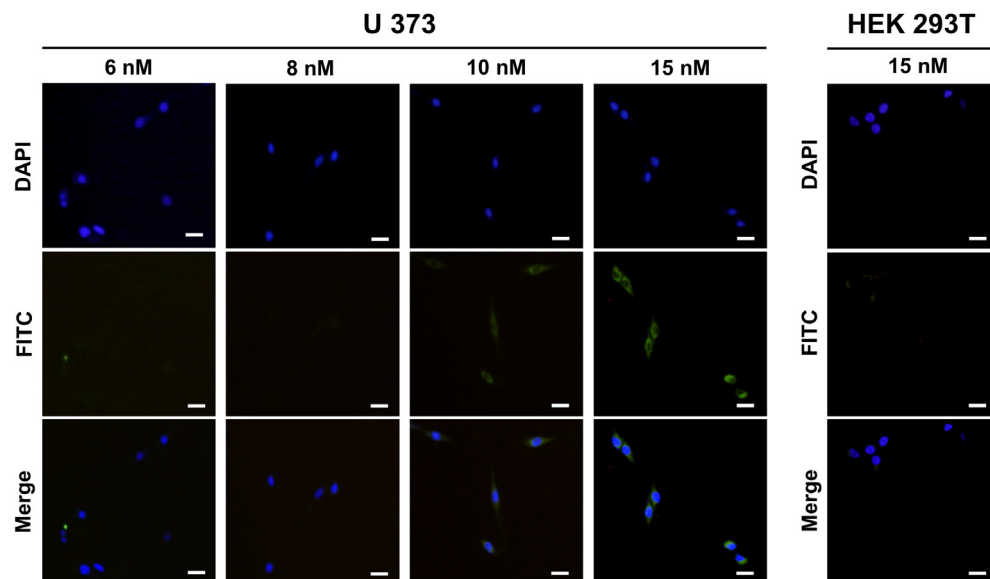


**Fig. 6.** Immunostaining results of U373 cells under live cell conditions. (a) The indicated concentration of GNP-PEG-CBP4 was incubated with the target cell for 8 h and then fluorescence images were acquired. HEK293T cells were also tested as a negative control. (b) Immunostaining using GNP-PEG-CBP4 (without FITC) and GNP-PEG-sc Peptide to analyze the specificity of imaging via active targeting of GNP-PEG-CBP4. Scale bar: 20  $\mu$ m.

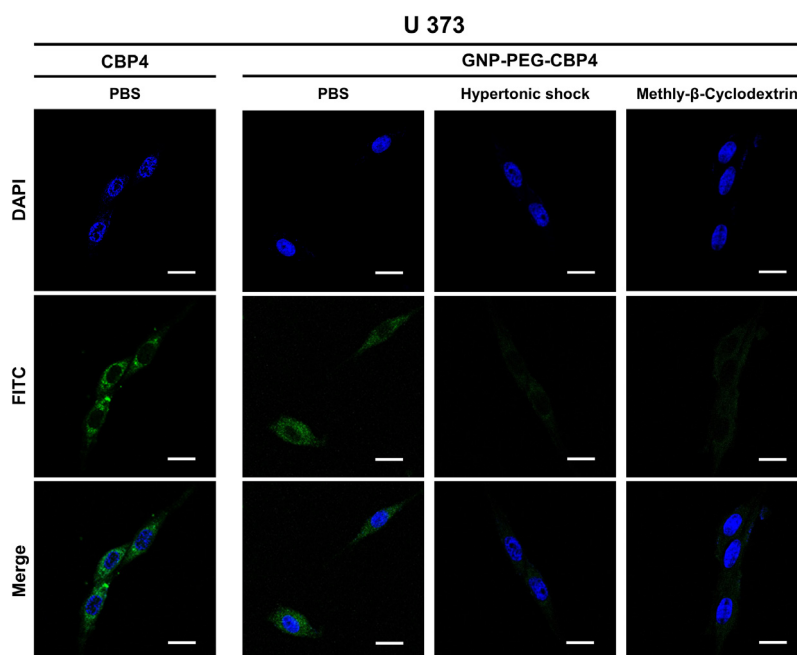


**Fig. 7.** Confocal imaging analysis using CBP4 and GNP-PEG-CBP4 to compare cellular localization via endocytosis. Hypertonic buffer and Methyl- $\beta$ -Cyclodextrin were used as an inhibitor of CD133 mediated endocytosis. PBS buffer was used as a baseline normal condition. Scale bar: 20  $\mu$ m.

CBP4 fluorescence was observed from intracellular sites of the target cell. This implies that the receptor-mediated endocytosis was induced by binding interaction of CBP4 with the target CD133 on U373 cell (Fig. 1). Furthermore, cell viability testing revealed that CBP4 possessed biocompatibility when internalized to the cytosol (Fig. S7).

Gold nanoparticles (GNPs) were used as a quencher of the CBP4 fluorescence. To conjugate the CBP4 and the GNPs, we first coated the GNPs using polyethylene glycol and optimized their physico-chemical stability (Fig. 2). In the presence of EDC/NHS cross linker, the additional primary amine residue of CBP4 was linked to the carboxyl terminus of GNP-PEG; this cross reaction had 70–80%

conjugation efficiency (Fig. 3). The polyethylene glycol (2000 Da) surface coating of the GNPs was approximately 2–3 nm thick according to random coil modeling [46]. In addition, the 12-mer peptide is of 0.5–1 nm height in normal conditions [47]. Accordingly, the maximum distance for the quenching effect was approximately 3–4 nm, an appropriate distance for highly efficient quenching. Indeed, highly efficient quenching was observed between GNP and CBP4; the fluorescence of FITC on CBP4 was fully quenched by GNP and had a stable ‘signal-off’ state in the solution phase (Fig. 4). Glutathione (GSH), which is abundantly present in the cytosol of cancer cells, was used as the stimulus agent in this study. According to a displacement assay, in acidic conditions

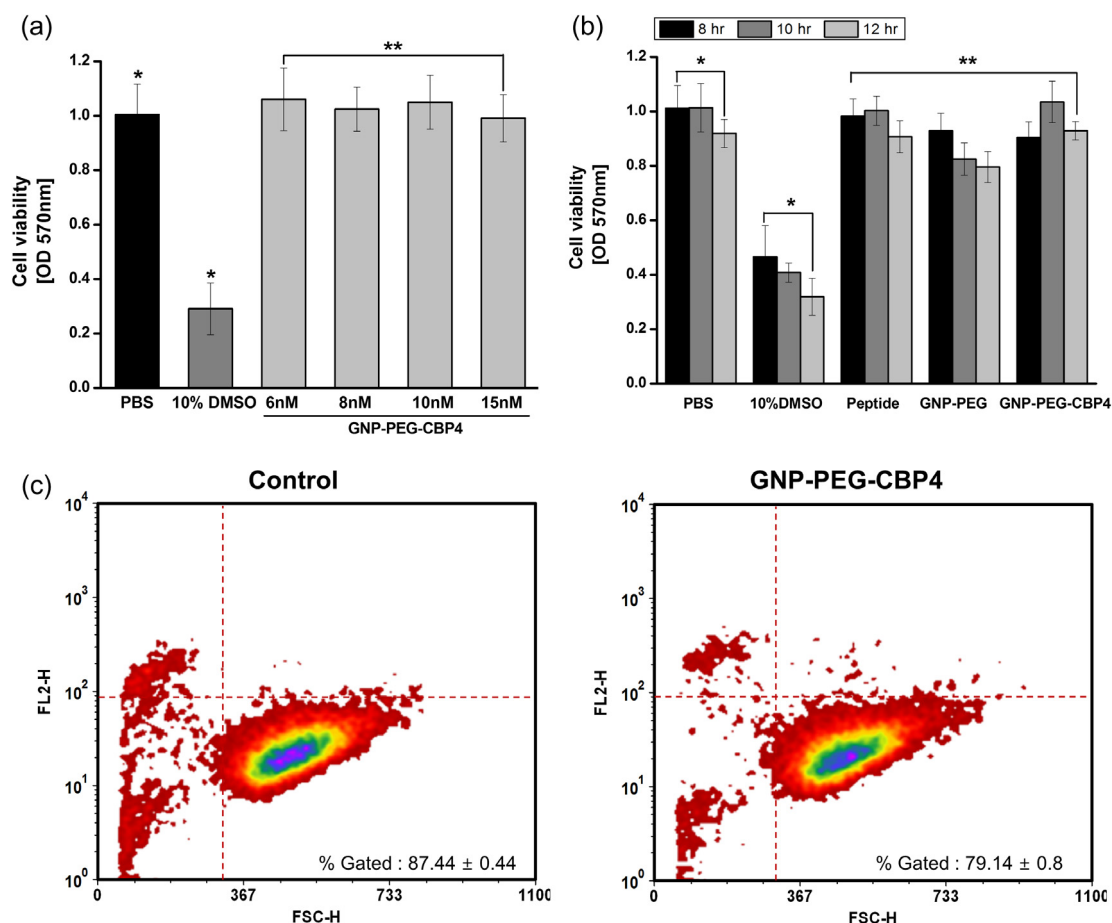


**Fig. 8.** In vitro cytotoxicity evaluation of GNP-PEG-CBP4 via MTT assay and PI staining. (a) Cell viability using GNP-PEG-CBP4 in an 8 h incubation condition and (b) in a time-dependent manner using CBP4 (1  $\mu$ M), GNP-PEG (15 nM) and GNP-PEG-CBP4 (15 nM) via measurement of mitochondrial dehydrogenase activity. (c) PI stained the GNP-PEG-CBP4 treated U373 cell and analysis the cellular viability using FACS. Data are shown as the mean  $\pm$  SD ( $n = 3$ ). (\* $p < 0.05$ , \*\* $p < 0.005$ ).

(PBS, pH 6.0) the fluorescence intensity was higher than that in high-pH conditions (Fig. 5). In its reaction with GSH, the CBP4 in GNP-PEG-CBP4 was displaced by GSH, yielding a fluorescence signal and changing the complex to a 'signal-on' state. This result of pH-dependent displacement activity of GSH was correlated with those of thiol-disulfide exchange reaction mechanisms in cytosol [48]. In addition, the acidic conditions of cytosol in cancer cells have led to the idea of stimulus-responsive imaging agents based on GSH [49].

We also estimated the binding specificity of GNP-PEG-CBP4 to U373 cells. Under the conditions of 15 nM GNP-PEG-CBP4 and 8 h incubation time, the target U373 cells showed a fluorescence imaging response and the control HEK293T cells did not (Fig. S9). This result indicated that GNP-PEG-CBP4 specifically recognized the target CD133 and accumulated in the cellular cytosol. Moreover, when in the cytosol, GNP-PEG-CBP4 reacted with the abundant GSH (10–20 mM) during the incubation time, thereby switching its fluorescence signal on as a response to the GSH stimulus. In addition, CBP4 maintained its novel binding characteristics when conjugated in the particle, and played an important role in the highly specific active targeting of the U373 cell via recognition of CD133. (Fig. 6). These results were supported by confocal microscopy data demonstrating the efficacy of cellular internalization using GNP-PEG-CBP4 in live U373 cells under endocytic inhibition condition. The stimulus response of GNP-PEG-CBP4 was blocked under endocytic inhibition condition. (Fig. 7).

FRET-based quenching occurred on GNP-PEG-CBP4 localized on CD133 (ECD) because of the absence of the stimulatory reagent in

the extracellular region. Contrastingly, under the baseline condition, GNP-PEG-CBP4 yielded a recoverable fluorescence signal similar to that of CBP4 alone in cytosol. This result implies that GNP-PEG-CBP4 has an on-off fluorescence signal that depends on intracellular stimulus by GSH. To analyze the biocompatibility of GNP-PEG-CBP4, we measured the cell viability using MTT and a PI staining method on U373 glioma cells. The GNP-PEG-CBP4 clearly exhibited no cytotoxicity under various conditions (Fig. 8). Especially, the GNP-PEG-CBP4 yielded cell viability results comparable to those of PBS and CBP4 alone. Thus, GNP-PEG-CBP4 shows promise as a novel biocompatible imaging agent.

Overall, in the present study we characterized the quenching-based signal on-off mechanism well and showed that active targeting via CBP4 can contribute to the design of a stimulus-responsive imaging agent against brain glioblastoma. However, the blood brain barrier (BBB) and the blood-spinal cord barrier (BSCB) greatly restrict the delivery of diagnostic and therapeutic biomolecules into the brain. To effectively target brain tumors, the attachment of cell penetrating peptide (CPP) [50] onto particles is one way to overcome this limitation, and the intranasal administration was proposed to bypass the BBB [51]. In addition, the small size of GNP-PEG-CBP4 ( $\sim$ 20 nm) was effective for passage into the brain extracellular space [52].

Although the current system has limitations, the platform designed using peptide and nanoparticles can be successfully applied to the field of cancer diagnostics. Especially, we envision that peptides are better at targeting ligands than antibodies for nanoparticle conjugation, not only for keeping the overall size

small but also for fully taking advantage of the polyvalency effect. Peptide coated particles might be a promising tool for drug carrier systems to be able to measure and visualize the delivered efficiency at intracellular sites.

## 5. Conclusions

We have demonstrated a novel imaging agent based on a convergence technique using the small peptide of CBP4 conjugated with GNPs. CBP4 exhibits outstanding targeting efficiency despite its conjugation on the particle surface. Furthermore, our 'signal on-off' imaging system using GNPs as the quencher allowed successful visualization of the target cell as a response to the stimulus agent GSH. This target-specific on-off property can be a useful tool for various cancer imaging and drug carrier systems.

## Acknowledgement

This research was supported by the Converging Research Center Program funded by the Ministry of Science, ICT & Future Planning (Project No. 2015054348) and a National Research Foundation of Korea (NRF) grant funded by the Korean Government (MSIP) (No. 20150000001213).

## Appendix A. Supplementary data

Supplementary data associated with this article can be found, in the online version, at <http://dx.doi.org/10.1016/j.actbio.2016.10.009>.

## References

- [1] A. Omuro, L.M. DeAngelis, Glioblastoma and other malignant gliomas: a clinical review, *JAMA* 310 (2013) 1842–1850.
- [2] P.M. Costa, A.L. Cardoso, C. Nobrega, L.F. Pereira de Almeida, J.N. Bruce, P. Canoll, M.C. Pedrosa de Lima, MicroRNA-21 silencing enhances the cytotoxic effect of the antiangiogenic drug sunitinib in glioblastoma, *Hum. Mol. Genet.* 22 (2013) 904–918.
- [3] S.C. Formenti, S. Demaria, Combining radiotherapy and cancer immunotherapy: a paradigm shift, *J. Natl. Cancer Inst.* 105 (2013) 256–265.
- [4] F.A. Dungey, K.W. Caldecott, A.J. Chalmers, Enhanced radiosensitization of human glioma cells by combining inhibition of poly(ADP-ribose) polymerase with inhibition of heat shock protein 90, *Mol. Cancer Ther.* 8 (2009) 2243–2254.
- [5] V. Tirino, V. Desiderio, F. Paino, A. De Rosa, F. Papaccio, M. La Noce, M. La Noce, L. Laino, F. De Francesco, G. Papaccio, Cancer stem cells in solid tumors: an overview and new approaches for their isolation and characterization, *FASEB J.* 27 (2013) 13–24.
- [6] K. Chen, Y.H. Huang, J.L. Chen, Understanding and targeting cancer stem cells: therapeutic implications and challenges, *Acta Pharmacol. Sin.* 34 (2013) 732–740.
- [7] P.C. Hermann, S. Bhaskar, M. Cioffi, C. Heeschen, Cancer stem cells in solid tumors, *Semin. Cancer Biol.* 20 (2010) 77–84.
- [8] S.K. Singh, C. Hawkins, I.D. Clarke, J.A. Squire, J. Bayani, T. Hide, R.M. Henkelman, M.D. Cusimano, P.B. Dirks, Identification of human brain tumour initiating cells, *Nature* 432 (2004) 396–401.
- [9] P. Brescia, B. Ortensi, L. Fornasari, D. Levi, G. Broggi, G. Pelicci, CD133 is essential for glioblastoma stem cell maintenance, *Stem Cells* 31 (2013) 857–869.
- [10] R.K. Kim, Y. Suh, E. Hwang, K.C. Yoo, K.S. Choi, S. An, S.G. Hwang, I.G. Kim, M. Kim, H.J. Lee, S.J. Lee, PKCdelta maintains phenotypes of tumor initiating cells through cytokine-mediated autocrine loop with positive feedback, *Oncogene* (2015).
- [11] J. Pande, M.M. Szewczyk, A.K. Grover, Phage display: concept, innovations, applications and future, *Biotechnol. Adv.* 28 (2010) 849–858.
- [12] Y.A. Wang, X. Yu, S. Overman, M. Tsuboi, G.J. Thomas Jr., E.H. Egelman, The structure of a filamentous bacteriophage, *J. Mol. Biol.* 361 (2006) 209–215.
- [13] J. Wang, Y. Liu, T. Teesalu, K.N. Sugahara, V.R. Kotamraju, J.D. Adams, B.S. Ferguson, Q. Gong, S.S. Oh, A.T. Csordas, M. Cho, E. Ruoslahti, Y. Xiao, H.T. Soh, Selection of phage-displayed peptides on live adherent cells in microfluidic channels, *Proc. Natl. Acad. Sci. U.S.A.* 108 (2011) 6909–6914.
- [14] T. Teesalu, K.N. Sugahara, E. Ruoslahti, Tumor-penetrating peptides, *Front. Oncol.* 3 (2013) 216.
- [15] P.L. Hsiung, J. Hardy, S. Friedland, R. Soetikno, C.B. Du, A.P. Wu, P. Sahbaie, J.M. Crawford, A.W. Lowe, C.H. Contag, T.D. Wang, Detection of colonic dysplasia in vivo using a targeted heptapeptide and confocal microendoscopy, *Nat. Med.* 14 (2008) 454–458.
- [16] R. Seigneuric, J. Gobbo, P. Colas, C. Garrido, Targeting cancer with peptide aptamers, *Oncotarget* 2 (2011) 557–561.
- [17] M.A. Hahn, A.K. Singh, P. Sharma, S.C. Brown, B.M. Moudgil, Nanoparticles as contrast agents for in-vivo bioimaging: current status and future perspectives, *Anal. Bioanal. Chem.* 399 (2011) 3–27.
- [18] A.S. Thakor, J. Jokerst, C. Zavaleta, T.F. Massoud, S.S. Gambhir, Gold nanoparticles: a revival in precious metal administration to patients, *Nano Lett.* 11 (2011) 4029–4036.
- [19] B. Dubertret, M. Calame, A.J. Libchaber, Single-mismatch detection using gold-quenched fluorescent oligonucleotides, *Nat. Biotechnol.* 19 (2001) 365–370.
- [20] K. Saha, S.S. Agasti, C. Kim, X. Li, V.M. Rotello, Gold nanoparticles in chemical and biological sensing, *Chem. Rev.* 112 (2012) 2739–2779.
- [21] J. Wang, S. Achilefu, M. Nantz, K.A. Kang, Gold nanoparticle-fluorophore complex for conditionally fluorescing signal mediator, *Anal. Chim. Acta* 695 (2011) 96–104.
- [22] S.R. MacEwan, D.J. Callahan, A. Chilkoti, Stimulus-responsive macromolecules and nanoparticles for cancer drug delivery, *Nanomedicine* 5 (2010) 793–806.
- [23] N. Singh, A. Karambelkar, L. Gu, K. Lin, J.S. Miller, C.S. Chen, M.J. Sailor, S.N. Bhatia, Bioresponsive mesoporous silica nanoparticles for triggered drug release, *J. Am. Chem. Soc.* 133 (2011) 19582–19585.
- [24] J. Su, F. Chen, V.L. Cryns, P.B. Messersmith, Catechol polymers for pH-responsive, targeted drug delivery to cancer cells, *J. Am. Chem. Soc.* 133 (2011) 11850–11853.
- [25] P. Sun, D. Zhou, Z. Gan, Novel reduction-sensitive micelles for triggered intracellular drug release, *J. Control. Release* 155 (2011) 96–103.
- [26] S. Chakravarthi, C.E. Jessop, N.J. Bulleid, The role of glutathione in disulphide bond formation and endoplasmic-reticulum-generated oxidative stress, *EMBO Rep.* 7 (2006) 271–275.
- [27] J.M. Estrela, A. Ortega, E. Obrador, Glutathione in cancer biology and therapy, *Crit. Rev. Clin. Lab. Sci.* 43 (2006) 143–181.
- [28] L. Li, Nurunnabi, Nafujjaman, Y.K. Lee, K.M. Huh, GSH-mediated photoactivity of pheophorbide a-conjugated heparin/gold nanoparticle for photodynamic therapy, *J. Control. Release* 171 (2013) 241–250.
- [29] Q.L. Wang, S.R. Wang, Y. Ding, K.J. Peng, X. Lin, X.R. Qiao, Y.L. Liu, C.H. Wu, Age-related changes of the redox state of glutathione in plasma, *Chin. Med. J.* 118 (2005) 1560–1563.
- [30] M.P. Gamcsik, M.S. Kasibhatla, S.D. Teeter, O.M. Colvin, Glutathione levels in human tumors, Biomarkers: Biochemical Indicators of Exposure, Response, and Susceptibility to Chemicals 17 (2012) 671–691.
- [31] S. Akella, C.K. Mitra, Electrochemical studies of glucose oxidase immobilized on glutathione coated gold nanoparticles, *Indian J. Biochem. Biophys.* 44 (2007) 82–87.
- [32] G.F. Luo, W.H. Chen, Y. Liu, Q. Lei, R.X. Zhuo, X.Z. Zhang, Multifunctional enveloped mesoporous silica nanoparticles for subcellular co-delivery of drug and therapeutic peptide, *Sci. Rep.* 4 (2014) 6064.
- [33] D.Y. Cho, S.Z. Lin, W.K. Yang, H.C. Lee, D.M. Hsu, H.L. Lin, C.C. Chen, C.L. Liu, W. Y. Lee, L.H. Ho, Targeting cancer stem cells for treatment of glioblastoma multiforme, *Cell Transplant.* 22 (2013) 731–739.
- [34] N. Oka, A. Soeda, A. Inagaki, M. Onodera, H. Maruyama, A. Hara, T. Kunisada, H. Mori, T. Iwana, VEGF promotes tumorigenesis and angiogenesis of human glioblastoma stem cells, *Biochem. Biophys. Res. Commun.* 360 (2007) 553–559.
- [35] D. Kumar, B.J. Meenan, D. Dixon, Glutathione-mediated release of Bodipy(R) from PEG cofunctionalized gold nanoparticles, *Int. J. Nanomed.* 7 (2012) 4007–4022.
- [36] A. Inagaki, A. Soeda, N. Oka, H. Kitajima, J. Nakagawa, T. Motohashi, T. Kunisada, T. Iwama, Long-term maintenance of brain tumor stem cell properties under at non-adherent and adherent culture conditions, *Biochem. Biophys. Res. Commun.* 361 (2007) 586–592.
- [37] J.E. Heuser, R.G. Anderson, Hypertonic media inhibit receptor-mediated endocytosis by blocking clathrin-coated pit formation, *J. Cell Biol.* 108 (1989) 389–400.
- [38] C.L. Chen, W.H. Hou, I.H. Liu, G. Hsiao, S.S. Huang, J.S. Huang, Inhibitors of clathrin-dependent endocytosis enhance TGFbeta signaling and responses, *J. Cell Sci.* 122 (2009) 1863–1871.
- [39] K. Sato, K. Hosokawa, M. Maeda, Non-cross-linking gold nanoparticle aggregation as a detection method for single-base substitutions, *Nucleic Acids Res.* 33 (2005) e4.
- [40] H. He, C. Xie, J. Ren, Nonbleaching fluorescence of gold nanoparticles and its applications in cancer cell imaging, *Anal. Chem.* 80 (2008) 5951–5957.
- [41] Y.W. Chen, G.G. Liou, H.B. Pan, H.H. Tseng, Y.T. Hung, C.P. Chou, Specific detection of CD133-positive tumor cells with iron oxide nanoparticles labeling using noninvasive molecular magnetic resonance imaging, *Int. J. Nanomed.* 10 (2015) 6997–7018.
- [42] D. Lowe, K. Dudgeon, R. Rouet, P. Schofield, L. Jeremias, D. Christ, Aggregation, stability, and formulation of human antibody therapeutics, *Adv. Protein Chem. Struct. Biol.* 84 (2011) 41–61.
- [43] F. Iacopino, C. Angelucci, R. Piacentini, F. Biamonte, A. Mangiola, G. Maira, C. Grassi, G. Sica, Isolation of cancer stem cells from three human glioblastoma cell lines: characterization of two selected clones, *PLoS One* 9 (2014) e105166.
- [44] E. Bourseaue-Guilmain, A. Griveau, J.P. Benoit, E. Garcion, The importance of the stem cell marker prominin-1/CD133 in the uptake of transferrin and in iron metabolism in human colon cancer Caco-2 cells, *PLoS One* 6 (2011) e25515.

- [45] D. Vercauteren, R.E. Vandenbroucke, A.T. Jones, J. Rejman, J. Demeester, S.C. De Smedt, N.N. Sanders, K. Braeckmans, The use of inhibitors to study endocytic pathways of gene carriers: optimization and pitfalls, *Mol. Ther.* 18 (2010) 561–569.
- [46] M. Oishi, A. Tamura, T. Nakamura, Y. Nagasaki, A smart nanoprobe based on fluorescence-quenching PEGylated nanogels containing gold nanoparticles for monitoring the response to cancer therapy, *Adv. Funct. Mater.* 19 (2009) 827–834.
- [47] T. Scherf, R. Kasher, M. Balass, M. Fridkin, S. Fuchs, E. Katchalski-Katzir, A beta-hairpin structure in a 13-mer peptide that binds alpha-bungarotoxin with high affinity and neutralizes its toxicity, *Proc. Natl. Acad. Sci. U.S.A.* 98 (2001) 6629–6634.
- [48] M. Deponte, Glutathione catalysis and the reaction mechanisms of glutathione-dependent enzymes, *Biochim. Biophys. Acta* 1830 (2013) 3217–3266.
- [49] Y. Kato, S. Ozawa, C. Miyamoto, Y. Maehata, A. Suzuki, T. Maeda, Y. Baba, Acidic extracellular microenvironment and cancer, *Cancer Cell Int.* 13 (2013) 89.
- [50] S. Lim, W.J. Kim, Y.H. Kim, S. Lee, J.H. Koo, J.A. Lee, H. Yoon, D.H. Kim, H.J. Park, H.M. Kim, H.G. Lee, J. Yun Kim, J.U. Lee, J. Hun Shin, L. Kyun Kim, J. Doh, H. Kim, S.K. Lee, A.L. Bothwell, M. Suh, J.M. Choi, DNP2 is a blood-brain barrier-permeable peptide enabling ctCTLA-4 protein delivery to ameliorate experimental autoimmune encephalomyelitis, *Nat. Commun.* 6 (2015).
- [51] S.V. Dhuria, L.R. Hanson, W.H. Frey 2nd, Intranasal delivery to the central nervous system: mechanisms and experimental considerations, *J. Pharm. Sci.* 99 (2010) 1654–1673.
- [52] R.G. Thorne, C. Nicholson, In vivo diffusion analysis with quantum dots and dextrans predicts the width of brain extracellular space, *Proc. Natl. Acad. Sci. U.S.A.* 103 (2006) 5567–5572.